PROCEEDINGS, TOUGH Symposium 2006
Lawrence Berkeley National Laboratory, Berkeley, California, May 15–17, 2006

MODELING GEOLOGIC STORAGE OF CARBON DIOXIDE: COMPARISON OF NON-HYSTERETIC AND HYSTERETIC CHARACTERISTIC CURVES

Christine Doughty

Lawrence Berkeley National Laboratory
#1 Cyclotron Rd, MS 90-1116
Berkeley, California, 94708, USA
e-mail: cadoughty@lbl.gov

ABSTRACT

TOUGH2 models of geologic storage of carbon dioxide (CO_2) in brine-bearing formations use characteristic curves to represent the interactions of non-wetting-phase CO_2 and wetting-phase brine. When a problem includes both injection of CO_2 (a drainage process) and its subsequent post-injection evolution (a combination of drainage and wetting), hysteretic characteristic curves are required to correctly capture the behavior of the CO_2 plume. In the hysteretic formulation, capillary pressure and relative permeability depend not only on the current grid-block saturation, but also on the history of the saturation in the grid block. For a problem that involves only drainage or only wetting, a non-hysteretic formulation, in which capillary pressure and relative permeability depend only on the current value of the grid-block saturation, is adequate. For the hysteretic formulation to be robust computationally, care must be taken to ensure the differentiability of the characteristic curves both within and beyond the turning-point saturations where transitions between branches of the curves occur. Two example problems involving geologic CO_2 storage are simulated using non-hysteretic and hysteretic models, to illustrate the applicability and limitations of non-hysteretic methods: the first considers leakage of CO_2 from the storage formation to the ground surface, while the second examines the role of heterogeneity within the storage formation.

INTRODUCTION

TOUGH2 has been used extensively in the past few years to model geologic storage of CO_2 in brine-saturated formations. At depths commonly considered for CO_2 storage (>800 m), CO_2 primarily exists as a gas-like supercritical phase, which is the non-wetting phase, while some CO_2 dissolves in the brine, which is the wetting phase. Interactions between the two fluid phases are represented at the grid-block scale by characteristic curves, that is, capillary pressure and relative permeability functions. The simplest characteristic curves are non-hysteretic – the capillary pressure and relative permeabilities depend only on the local saturation at the current time. A more sophisticated approach is a hysteretic formulation, in which capillary pressure and relative permeabilities depend not only on the current value of the local saturation, but on the history of the local saturation and the process that is occurring: drainage (replacement of wetting phase with non-wetting phase) or wetting (replacement of non-wetting phase with wetting phase, also known as imbibition).

The use of hysteretic characteristic curves is not so critical for the simulation of CO_2 injection periods when the plume is continuously growing, because all locations follow the primary drainage branch of the capillary pressure curve at all times, and this branch can be replicated using a non-hysteretic formulation. However, for post-injection periods, when the CO_2 plume moves upward and updip due to buoyancy forces, different locations experience drainage and wetting at different times, necessitating the use of a hysteretic formulation.

In the sections below, we outline the mathematical formulation of the hysteretic characteristic curves used for TOUGH2 modeling of CO_2 storage, then briefly describe some of the key numerical issues involved in implementing hysteretic functions into TOUGH2. Two example problems are presented to illustrate the effects of hysteretic characteristic curves, followed by some concluding remarks.

HYSTERETIC CHARACTERISTIC CURVES

Together, capillary pressure P_c and relative permeabilities k_{rl} and k_{rg} are known as characteristic curves; they control the way the liquid (wetting) phase and gas (non-wetting) phases interact. In a non-hysteretic model, the characteristic curves are single-valued functions of the current grid-block saturation. In contrast, in a hysteretic model, P_c, k_{rl}, and k_{rg} depend not only on the saturation of the grid block, but also on the history of the saturation of the grid block. Some parameters within the characteristic curve functions depend only on the process (drainage or imbibition) that is occurring, so it is convenient to subdivide the characteristic curves into drainage curves and wetting curves. Other parameters depend on the value of the saturation when the grid block makes a transition from drainage to imbibition or vice versa, the so-called turning point saturations. Because turning-point saturations differ among all grid blocks, these parameters do as well.

The most critical parameter in the latter category is the residual gas saturation, denoted S_{gr}^{Δ}, which is the saturation below which gas is immobile (i.e., the saturation below which immiscible CO_2 is trapped). Under drainage conditions, $S_{gr}^{\Delta} = 0$, but for imbibition, S_{gr}^{Δ} increases as the turning-point saturation between the drainage curve and wetting curve, denoted S_l^{Δ}, decreases. Thus, grid blocks that once contained the most CO_2 are those which trap the most CO_2.

Suppose we begin with a brine-saturated formation ($S_l = 1$) and inject immiscible CO_2. As CO_2 reaches each grid block, multiphase flow begins using a P_c known as the primary drainage curve. Whenever liquid saturation increases in a given grid block, a transition is made to the first-order scanning wetting curve, which is interpolated between the primary drainage curve and the so-called primary wetting curve, using the value of S_l^{Δ}. If liquid saturation decreases again, a transition is made to the second-order scanning drainage curve, again obtained by interpolation, which is followed until either (a) liquid saturation drops below its previous minimum value, S_l^{Δ}, at which point the primary drainage curve is again followed, or (b) liquid saturation again increases, at which point a transition is made to a higher-order scanning wetting curve. Figure 1 illustrates some typical hysteretic capillary pressure paths followed during a drainage/wetting sequence.

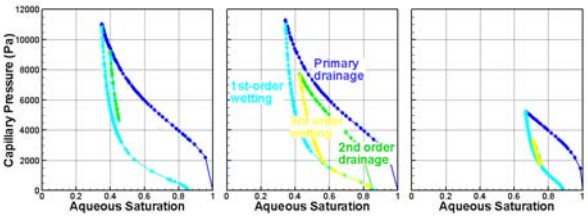

Figure 1. Hysteretic capillary pressure paths for scenario (a) (left frame) and scenario (b) described in text. Each path begins at S_l=1, P_c=0.

The primary drainage and primary wetting curves are based on the van Genuchten (1980) capillary pressure function

$$P_c = -\frac{1}{\alpha^{\gamma}}\left[\left(\frac{S_l - S_{l\min}}{1 - S_{gr}^{\Delta} - S_{l\min}}\right)^{-\left(\frac{n^{\gamma}}{n^{\gamma}-1}\right)} - 1\right]^{(1/n^{\gamma})}, \qquad (1)$$

where γ denotes the branch (d for drainage, w for wetting) of the capillary pressure curve and α, $S_{l\min}$, and n are fitting parameters. For both primary and scanning drainage curves, S_{gr}^{Δ}=0. For wetting curves, S_{gr}^{Δ} is given by a modified version of the well-known Land (1969) equation as

$$S_{gr}^{\Delta} = \frac{(1 - S_l^{\Delta})}{1 + [1/S_{gr\max} - 1/(1 - S_{lr})](1 - S_l^{\Delta})}, \qquad (2)$$

where S_{lr} is the residual liquid saturation (the saturation below which the liquid phase is immobile, assumed to be a constant rock property), S_l^{Δ} is the turning-point saturation for the transition from the primary drainage curve to the first-order wetting scanning curve, and $S_{gr\max}$ is taken as a function of porosity ϕ, obtained by fitting a wide range of sandstone data from the petroleum literature (M. Holtz, personal communication, 2002; Holtz, 2005)

$$S_{gr\max} = -0.3136 * \ln(\phi) - 0.1334. \qquad (3)$$

Note from Equation (2) that when $S_l^{\Delta} = S_{lr}$ (complete drainage of the medium before wetting begins), $S_{gr}^{\Delta} = S_{gr\max}$ and that when $S_l^{\Delta} \sim 1$ (only slight drainage before wetting begins), $S_{gr}^{\Delta} \sim 0$.

All together, four classes of capillary pressure curves are defined: the primary drainage and wetting curves, the first-order wetting scanning curve, the second-order scanning drainage curve, and the third-order scanning wetting curve. Details of the interpolation procedure used to determine the scanning drainage and wetting curves are not reproduced here; they are based on the dependent domain theory of Mualem (1984) and their implementation in TOUGH2 is fully described in Finsterle et al. (1998) and Niemi and Bodvarsson (1988).

The relative permeability functions also include hysteretic effects arising from the trapped component of the gas phase that develops during wetting. These functions are taken from Parker and Lenhard (1987) and Lenhard and Parker (1987), who adapted them from the non-hysteretic expressions of van Genuchten (1980). As implemented in TOUGH2, the relative permeability functions are

$$k_{rl} = \sqrt{\bar{S}_l}\left[1 - \left(1 - \frac{\bar{S}_{gt}}{1 - \bar{S}_l^{\Delta}}\right)\left(1 - (\bar{S}_l + \bar{S}_{gt})^{1/m}\right)^m - \left(\frac{\bar{S}_{gt}}{1 - \bar{S}_l^{\Delta}}\right)\left(1 - (\bar{S}_l^{\Delta})^{1/m}\right)^m\right]^2 \qquad (4)$$

$$k_{rg} = (1 - \bar{S}_l - \bar{S}_{gt})^{1/3}\left(1 - (\bar{S}_l + \bar{S}_{gt})^{1/m}\right)^m, \qquad (5)$$

where $\bar{S}_l$ and $\bar{S}_l^{\Delta}$ are effective values of liquid saturation S_l and turning point liquid saturation S_l^{Δ}, respectively, normalized with respect to irreducible liquid-phase saturation S_{lr}:

$$\bar{S}_l = \frac{S_l - S_{lr}}{1 - S_{lr}} \tag{6}$$

$$\bar{S}_l^{\Delta} = \frac{S_l^{\Delta} - S_{lr}}{1 - S_{lr}} . \tag{7}$$

The parameter $\bar{S}_{gt}$ is the effective value of the trapped gas-phase saturation, which is given by

$$\bar{S}_{gt} = \frac{S_{gr}^{\Delta}(S_l - S_l^{\Delta})}{(1 - S_{lr})(1 - S_l^{\Delta} - S_{gr}^{\Delta})} . \tag{8}$$

NUMERICAL MODEL DEVELOPMENT

The hysteretic capillary pressure functions shown above were implemented in TOUGH in the late 1980's (Niemi and Bodvarsson, 1988) and hysteretic relative permeability functions were added to TOUGH2 (within iTOUGH2) about ten years later (Finsterle et al., 1998). However, the hysteretic model was not numerically efficient enough to be used for 2D or 3D CO_2 sequestration problems. One crucial modification that we made is to ensure that capillary pressure and relative permeability functions are continuous and differentiable within and beyond the turning-point saturations that bound the different branches of the curves. This is required because actual saturations may fall beyond the turning-point values due to dissolution of CO_2 or numerical effects. Additionally, an option has been added to delay branch transitions to the end of the time step. This has the effect of making the fully implicit time-stepping normally employed by TOUGH2 partially explicit. With these modifications, hysteretic simulations are computationally competitive with non-hysteretic simulations.

APPLICATIONS

Two problems related to CO_2 sequestration are simulated using both hysteretic and non-hysteretic formulations for characteristic curves. The first problem considers leakage of CO_2 from the storage formation to the ground surface, while the second examines the role of heterogeneity within the storage formation. The TOUGH2 equation of state package used for the present work is ECO2 (Pruess and Garcia, 2002), which considers water, CO_2, and NaCl. Thermodynamic conditions include super- as well as sub-critical CO_2, but for sub-critical conditions, ECO2 does not distinguish liquid and gaseous CO_2, and associated phase changes cannot be represented. Thus for sub-critical conditions encountered between the storage formation and the ground surface for the leakage problem, ECO2 can only model flow paths that do not cross the saturation line. This can be accomplished by choosing a relatively warm surface temperature to keep the geothermal gradient on the gas side of the saturation line, and considering slow enough flows so that the CO_2 plume remains in near thermodynamic equilibrium with its surroundings, and thus remains close to the geothermal gradient.

Leakage from Formation to Surface

The model for this study is shown in Figure 2. CO_2 is injected into a porous formation 100 m thick located at a depth of 1000 m. The porosity of the formation is 28%, horizontal permeability is 200 md, and vertical permeability is 100 md. The base of the model is a closed boundary. Above the porous formation is an overburden, which extends to the surface. A range of properties has been considered for the overburden (Doughty and Myer, 2006), to study the fate of leaking CO_2 plumes, but here we just consider an overburden with the same properties as the storage formation itself.

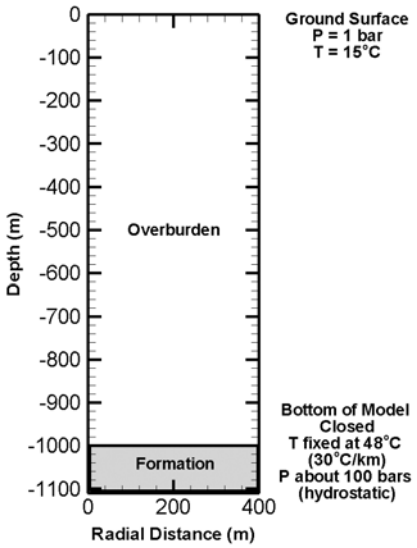

Figure 2. Schematic diagram of the first 400 m of the axisymmetric model for the leakage problem.

The numerical simulations were carried out using a 2D axisymmetric model composed of 61 layers each containing 41 grid blocks. All grid blocks are 20 m thick except for a few layers near the surface, which are thinner to better resolve surface arrival time. Radial grid block extent is 20 m out to a distance of 600 m, after which it steadily increases to produce an infinite-acting model.

Table 1 summarizes the material properties for the hysteretic model. Initially, the brine saturation is 100% everywhere in the model, pore pressure is hydrostatic with a pressure of 1 bar at the surface, and temperature follows the geothermal gradient of 30°C/km, with the temperature at the surface and base of the model held constant at 15°C and 48°C, respectively. The salinity of the pore water is assumed to be 100,000 ppm.

Table 1. Material properties for hysteretic model for leakage example.

Property	Value
Porosity ϕ	0.28
Horizontal Permeability (md)	200
Vertical Permeability (md)	100
Relative Permeability Parameters	
M	0.92
S_{lr}	0.30
S_{grmax}	0.25
Capillary Pressure Parameters	
$1/\alpha$ (bars)	0.133
N	1.7
S_{lmin}	0.03

The numerical simulations begin with injection of 900,000 tons of CO_2 into the porous formation at a constant rate of 30,000 tons per day for 30 days. This quantity of CO_2 corresponds roughly to the emissions of a 1,000 MW coal fired power plant for 30 days. After injection stops, the only driving force in the model tending to cause movement of the CO_2 is buoyancy. Simulations continue for 1,000 years.

In addition to the hysteretic model, two non-hysteretic models were also used for the leakage example problem. The non-hysteretic models use cubic relative permeability functions and the van Genuchten (1980) capillary pressure function. The first case has a large residual liquid saturation and a small residual gas saturation (S_{lr}=0.3, S_{gr}=0.05), which is believed to be appropriate for CO_2 injection periods, and creates a "slippery" CO_2 plume that moves easily through the formation with little trapping. The second case has a small residual liquid saturation and a large residual gas saturation (S_{lr}=0.1, S_{gr}=0.3), which is believed to be appropriate for the trailing edge of the CO_2 plume during the post-injection period, and produces a "sticky" CO_2 plume that traps substantial amounts of CO_2 as it moves.

Figure 3 shows snapshots of the free-phase CO_2 plumes at a series of times during the 1,000-year simulation period for the two non-hysteretic cases. Below depths of 700 m, the CO_2 is supercritical whereas above 700 m the CO_2 is gaseous. The fate of the CO_2 is very different for the two cases: the slippery plume reaches the surface within 10 years and most of the CO_2 escapes within 100 years, whereas the sticky plume never reaches the surface and remains entirely trapped indefinitely.

Figure 4 shows the CO_2 plume development for the hysteretic model. During the one-month injection period, the slippery non-hysteretic model and hysteretic model give similar results. Thereafter, neither non-hysteretic model fully captures the dynamics of plume evolution. The hysteretic model enables the leading edge of the plume, where drainage occurs and S_{gr} is small, to continue to advance, while the trailing edge of the plume, where imbibition occurs and S_{gr} is large, to remain largely trapped.

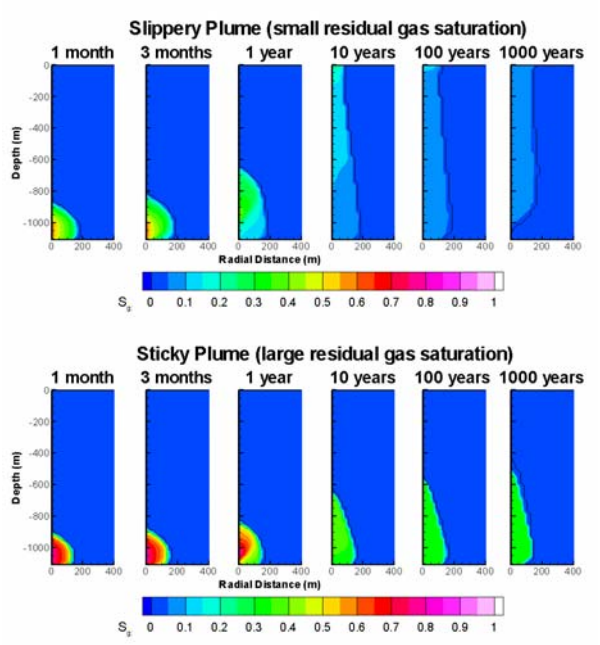

Figure 3. CO_2 plume evolution with non-hysteretic models. The single contour line shows S_g=0.

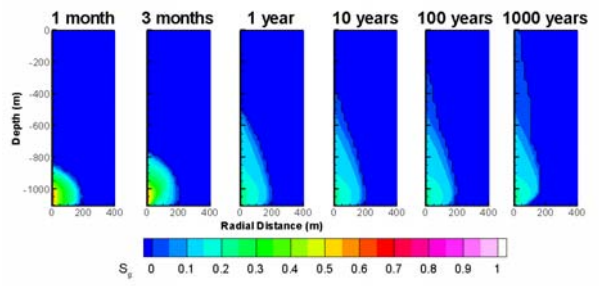

Figure 4. CO_2 plume with hysteretic model. The single contour line shows S_g=0.

Figure 5 shows the capillary pressure and relative permeability paths followed for several locations in the CO_2 plume using the hysteretic model. All paths begin at S_l = 1 along the primary drainage curve; the

transition to a wetting scanning curve occurs at S_l^{Δ} (shown by arrows); as |Pc| → 0 on the wetting curves, $S_l \rightarrow (1 - S_{gr}^{\Delta})$ (shown by black dots), with S_{gr}^{Δ} given by Equation (2). Thus grid blocks near the plume center, which get much drier during the injection period and therefore have a small S_l^{Δ}, have a much larger S_{gr}^{Δ}, and consequently trap more CO_2, than do grid blocks that the plume barely reaches.

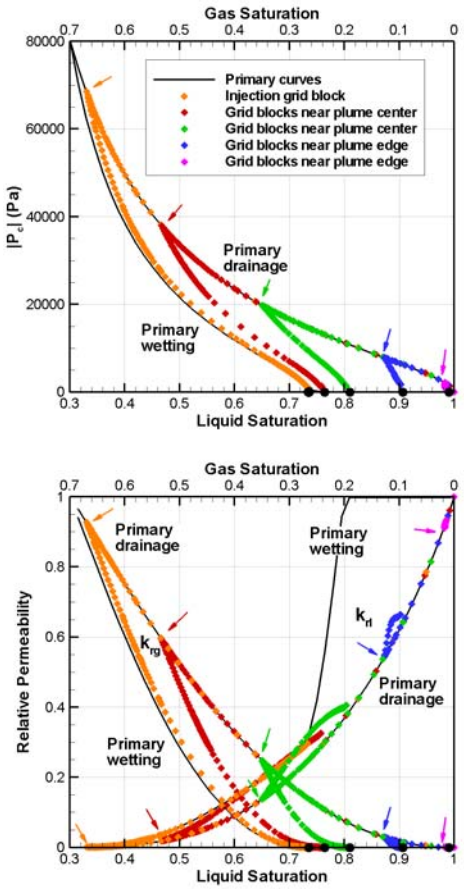

Figure 5. Hysteretic capillary pressure (top) and relative permeability (bottom) paths for several locations within CO_2 plume.

Figure 6 shows snapshots of the variable that identifies which branch of the capillary pressure curve is being followed: the primary drainage curve, the first-order wetting scanning curve, the second-order drainage scanning curve, or the third-order wetting scanning curve. At one month (the end of the injection period), the entire plume is draining. At three months, the upper half of the plume is draining and the lower half is wetting. By one year, most of the plume is wetting, with only a narrow band right at the leading edge draining. Note that as a plume spreads out, gas saturation decreases, which is equivalent to wetting. Thus, even in the absence of movement, a spreading plume will be wetting. At late times, the dominance of higher-order scanning curves indicates that saturation changes are small and tend to be oscillatory, as the bulk of the plume becomes immobile.

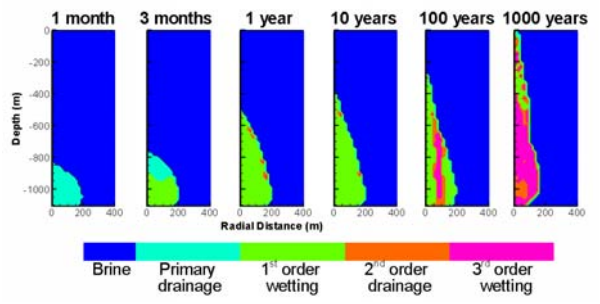

Figure 6. Branches of capillary pressure curves for hysteretic model.

Figure 7 shows the time variation of the mass fraction of CO_2 in different forms (mobile, immobile, and dissolved) integrated over the entire model, for all three cases. Mass fraction is calculated by dividing the mass present at each time by the total amount of CO_2 injected. The immiscible and dissolved fractions sum to the total fraction, and the mobile and immobile fractions sum to the immiscible fraction. The total fraction remains one if the CO_2 plume does not reach the surface. It is clear that neither non-hysteretic model successfully reproduces the behavior shown by the hysteretic model, in which the quantity of mobile CO_2 is high during the injection period, but rapidly drops after injection ceases.

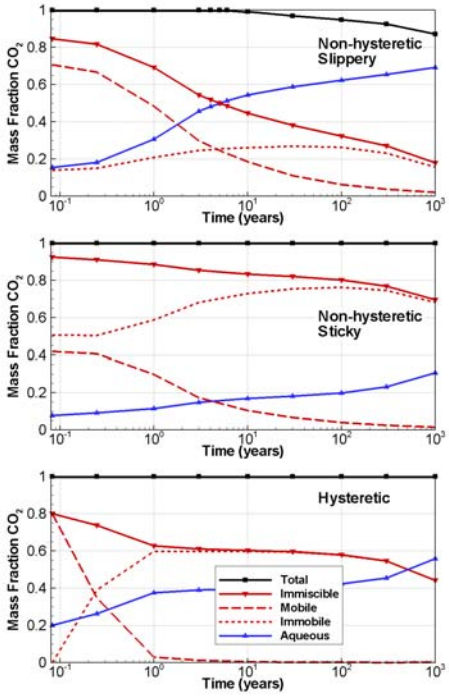

Figure 7. Mass fractions of CO_2 in various forms, integrated over the entire model.

Storage in a Heterogeneous Formation

The second example problem considers CO_2 injection and storage into a heterogeneous formation representing a fluvial-deltaic geology, consisting primarily of high-permeability sands, intercut with low-permeability shales (Figure 8). The 1 km by 1 km by 100 m thick model is created stochastically based on well logs and a simplified conceptualization of the regional depositional setting (Doughty and Pruess, 2004). It has 30 layers, each containing 400 grid blocks. The top and bottom boundaries are closed, and the lateral boundaries are held at constant pressure. Injection of CO_2 occurs through a single well penetrating the lower half of the formation at a constant rate of 2000 tons per day for a period of 20 years, after which the evolution of the CO_2 distribution is followed for 80 years. The present study uses the same characteristic curves as for the leakage problem described previously.

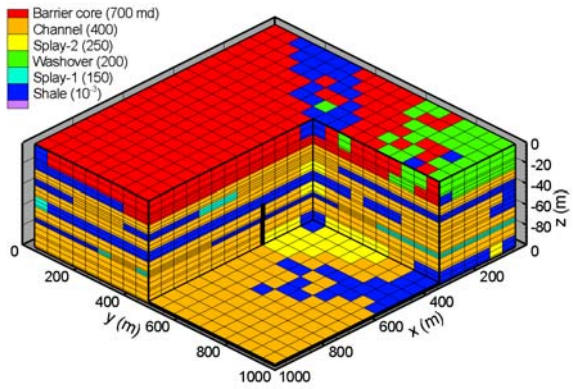

Figure 8. Cut-away view of the 3D model used for the heterogeneity problem. Horizontal permeability is shown for each material.

Figures 9 and 10 show the evolution of free-phase, supercritical CO_2 for non-hysteretic models for the slippery-plume case (small S_{gr}) and sticky-plume case (large S_{gr}), respectively.

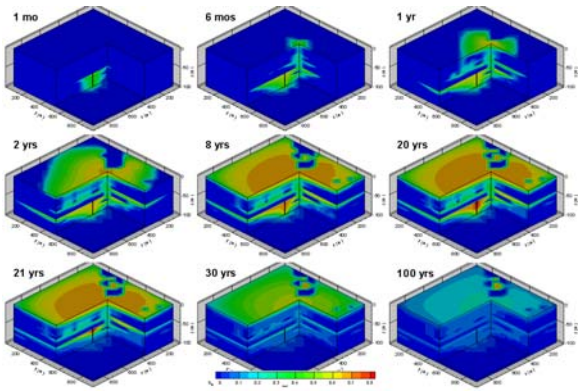

Figure 9. CO_2 plume evolution for non-hysteretic model, slippery-plume case (small S_{gr}.).

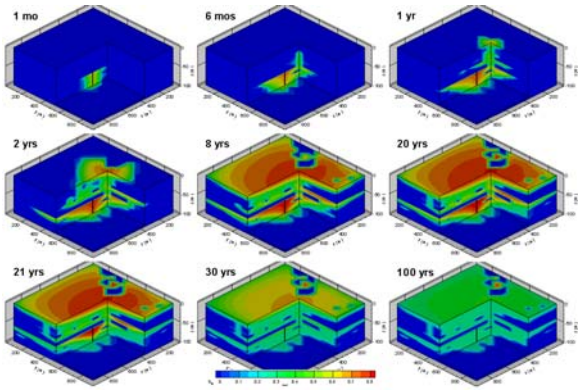

Figure 10. CO_2 plume evolution for non-hysteretic model, sticky-plume case (large S_{gr}).

It is clear that the choice of S_{gr} has a strong impact on CO_2 behavior throughout the injection and subsequent rest periods. During the injection period, the sticky plume is much more compact than the slippery plume, with significantly higher values of gas saturation. After injection ends, much more of the free-phases CO_2 exits through the lateral boundaries of the model for the slippery plume than for the sticky plume.

Figure 11 shows the CO_2 plume for the hysteretic model. During the injection period, the hysteretic and non-hysteretic slippery-plume case give similar results, but during the post-injection rest period neither non-hysteretic model agrees closely with the hysteretic model.

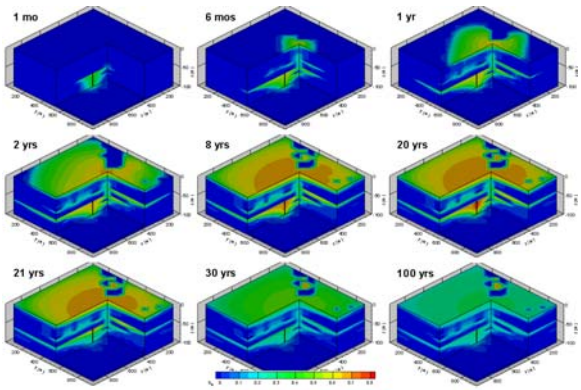

Figure 11. CO_2 plume evolution for hysteretic model.

Interestingly, there is one location where CO_2 remains trapped for all three cases, near the top of the model at about x=200 m, y=400 m, in a pocket of sand surrounded by low-permeability shale (compare Figures 8, 9, 10, and 11). This suggests that where structural trapping mechanisms exist, CO_2 becomes trapped regardless of multi-phase flow effects, and it is not so critical how characteristic curves are defined. Conversely, where structural trapping is

absent (or uncertain), properly representing multi-phase flow effects through characteristic curves becomes critical.

Figure 12 shows snapshots of the branches of the capillary pressure curve being followed for the hysteretic model, indicating which parts of the model are draining and wetting at various times. Unlike the leakage problem, here wetting begins before the injection period ends, a consequence of the subtle interplay between fluid flow and geologic heterogeneity. Most of the injection-period wetting occurs in the lower portion of the model, indicating that early in the injection period, flow into this region is greater than at later times. Thus, buoyancy-driven upward flow through gaps in the shale layers must increase with time. Such an increase is expected, as low-viscosity CO_2 replaces high-viscosity brine in the upper portion of the model.

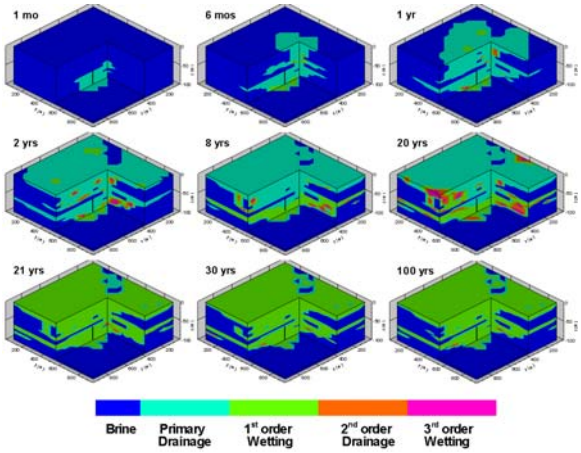

Figure 12. Branches of capillary pressure curves for hysteretic model.

Figure 13 shows the time variation of the mass of CO_2 in different forms (mobile, immobile, and dissolved) integrated over the entire model, for all three cases. A quasi-steady state develops by about 8 years into the injection period, in which CO_2 injection is approximately balanced by flow out the lateral boundaries of the model. Within about 10 years after the end of injection, the system again reaches a quasi-steady state, in which nearly all the CO_2 is immobile or dissolved. Neither non-hysteretic model produces the correct CO_2 masses throughout the entire simulation period. In particular, the non-hysteretic slippery-plume case underpredicts how much immiscible CO_2 can be stored, whereas the non-hysteretic sticky-plume case overpredicts it. Neither non-hysteretic model produces the sharp increase in immobile CO_2 that occurs when injection ends.

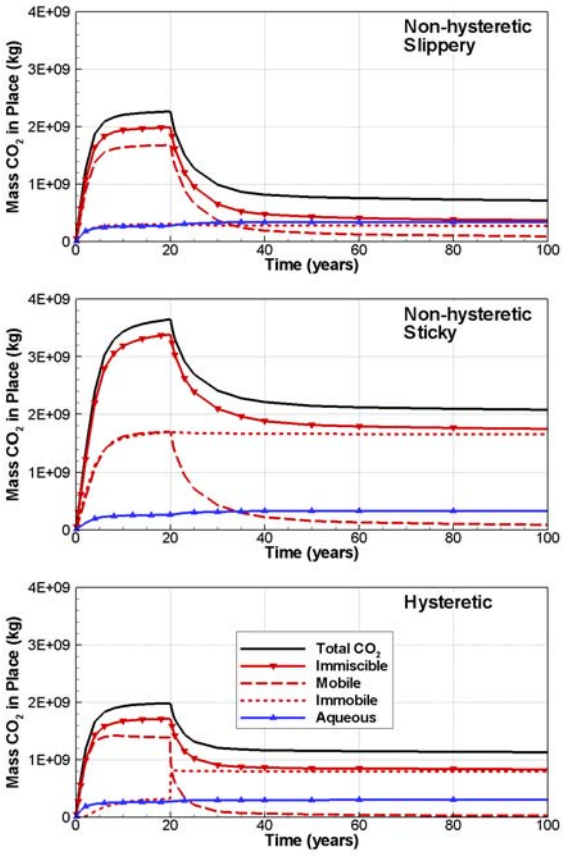

Figure 13. Mass of CO_2 in various forms, integrated over the entire model.

CONCLUSIONS

When a problem includes both injection of CO_2 (a drainage process) and its subsequent post-injection evolution (a combination of drainage and wetting), hysteretic models are required to correctly capture the behavior of the CO_2 plume. This is particularly true for geological settings where structural traps are absent or uncertain, and movement of CO_2 is controlled by the characteristic curves describing multi-phase flow effects.

ACKNOWLEDGMENT

The careful reviews of Stefan Finsterle and Curt Oldenburg are gratefully appreciated. This work was supported by the ZERT (Zero Emissions Research and Technology) and GEO-SEQ programs, through the Assistant Secretary for Fossil Energy, Office of Coal and Power Systems through the National Energy Technology Laboratory, and by Lawrence Berkeley National Laboratory under Department of Energy Contract No. DE-AC02-05CH1123.

REFERENCES

Doughty, C. and L.R. Myer, Scoping calculations on leakage of CO2 in geologic storage, in Science and technology of carbon sequestration, B. McPherson and E. Sundquist, Eds., American Geophysical Union, Washington, D.C., in press, 2006.

Doughty, C. and K. Pruess, Modeling supercritical carbon dioxide injection in heterogeneous porous media, *Vadose Zone Journal*, 3, 3, 837-847, 2004.

Finsterle, S., T.O. Sonnenborg, and B. Faybishenko, Inverse modeling of a multistep outflow experiment for determining hysteretic hydraulic properties, in K. Pruess, ed., Proceedings of the TOUGH workshop '98, Rep. LNBL-41995, Lawrence Berkeley National Laboratory, Berkeley, Calif., 1998.

Holtz, M. H., Reservoir characterization applying residual gas saturation modeling, example from the Starfak T1 reservoir, middle Miocene Gulf of Mexico, M.Sc. Thesis, University of Texas at Austin, 2005.

Land, C.S., Calculation of imbibition relative permeability for two- and three-phase flow from rock properties, *SPE Journal*, 9, 149-156, June 1969.

Lenhard, R.J. and J.C. Parker, A model for hysteretic constitutive relations governing multiphase flow, 2. Permeability-saturation relations, *Water Resources Research*, 23(12), 2197-2205, 1987.

Mualem, Y., A modified dependent domain theory of hysteresis, *Soil Science*, 137(5), 283-291, 1984.

Niemi, A. and G.S. Bodvarsson, Preliminary capillary hysteresis simulations in fractured rocks, Yucca Mountain, Nevada, *Journal of Contaminant Hydrology*, 3, 277-291, 1988.

Parker, J.C. and R.J. Lenhard, A model for hysteretic constitutive relations governing multiphase flow, 1. Saturation-pressure relations, *Water Resources Research*, 23(12) 2187-2196, 1987.

Pruess, K. and J. García, Multiphase flow dynamics during CO2 disposal into saline aquifers, *Environmental Geology*, 42, 282-295, 2002.

van Genuchten, M. Th., A closed-form equation for predicting the hydraulic conductivity of unsaturated soils, *Soil Science Society of America Journal*, 44(5), 892-898, 1980.